Astron. Astrophys. 335, 309–322 (1998)

ASTRONOMY AND ASTROPHYSICS

3-D magnetic configurations supporting prominences

II. The lateral feet as a perturbation of a twisted flux-tube

G. Aulanier[1], P. Démoulin[1], L. van Driel-Gesztelyi[1,2], P. Mein[1], and C. DeForest[3]

[1] Observatoire de Paris, Section Meudon, DASOP, URA 2080 (CNRS), F-92195 Meudon Principal Cedex, France
[2] Konkoly Observatory, Pf., H-1525 Budapest, Hungary
[3] NASA/Goddard SFC, Greenbelt, MD 20771, USA

Received 21 October 1997 / Accepted 9 March 1998

Abstract. In a previous paper we have shown that a twisted flux-tube is the most probable magnetic configuration supporting prominences. The model interprets many observations in a natural way (in particular the magnetic measurements in prominences and the chirality properties). Moreover, prominence feet appear as a direct consequence of the parasitic polarities present in the filament channel. Here we investigate further the link between feet and parasitic polarities by modelling explicitly these polarities. We show that the prominence lateral feet appear naturally, above secondary photospheric inversion lines and we describe the morphological change of feet as parasitic polarities evolve. This approach is applied to an observed filament in Hα with the MSDP on the German VTT (Tenerife) where SOHO/MDI magnetograms are available. We show that the shape of the prominence is defined by the distribution of the dips in the computed magnetic configuration. Then we analyse the topology of the magnetic field using the quasi-separatrix layers (QSLs) method. We describe the basic changes in the topology as the parasitic polarities evolve, in particular how the configuration pass from an OX to an OF topology. We find a correspondance between the computed QSLs and some of the chromospheric brightenings, observed around the feet of filaments in the y line (Ca II, 8542 Å). It confirms the deduced magnetic configuration and shows that energy release is present at a low level in the complex topology of the filament configuration.

Key words: magnetic fields – Sun: chromosphere – Sun: magnetic fields – Sun: prominences – Sun: filaments

1. Introduction

Prominences are composed of cold plasma suspended in the hot corona. They are observed in absorption on the disk, so they look like dark features in Hα . Their shape can be described as a main body, with underlying feet that can be seen when they are observed on the limb. The feet join the photosphere with a periodicity of a few tens of Mm, which is relevant of their connection with supergranules. Viewed on the disk from above, some lateral feet or barbs are also present. They often appear in pairs at both sides, shifted from one another. The typical evolution time of these feet go from a few hours to a day.

Filaments are always found above inversion lines of the vertical photospheric magnetic field. Their chromospheric environment is called filament channel. On each side of prominence, Hα fibrils are nearly parallel to the inversion line. This indicates a strong magnetic shear in the filament channel (Foukal 1971, Rompolt 1990). Eventually some fibrils can be darker, and seem to converge to bright regions above photospheric magnetic polarities. These groups of fibrils are called plagettes. Another remarkable feature is the change of orientation of the fibrils as one looks far away from the filament. These fibrils form a fishbone-like structure at the border of the filament channel (Filippov 1994). It is indirect evidence of a twisted flux-tube along the filament body.

The hydrostatic pressure scale height in prominences is about 300 km, though their height can go up to 50,000 km. Furthermore, their velocity pattern is not consistent with plasma flowing down, as there are not only downwards, but also upwards and horizontal motions. The observed plasma velocities are usually a few $\mathrm{km\,s^{-1}}$(e.g. Schmieder, 1990), which is far from the typical free fall velocity (several $10\,\mathrm{km\,s^{-1}}$). This implies that the support against gravity, and probably the global evolution of filaments, is driven by the magnetic field.

Hanle-effect measurements of the magnetic field inside prominences constrain the description of the field in several ways. The field is nearly horizontal (Athay et al. 1983), and its strength is nearly homogeneous, though it slightly increases with height (Leroy 1989). This is consistent with the characteristics of dips in the field lines (Bommier et al. 1986, 1994). Hanle measurements also highlight that a large majority of prominences are inverse type (Leroy et al. 1984 and Bommier & Leroy 1997). This refers to the direction of the magnetic field inside them, which is opposite to the one of a simple arcade rooted in the main bipolar photospheric field.

The persistence and stability of the main body of filaments naturally leads to consider them to be in global magnetohydrostatic equilibrium. The value of β for the plasma in the promi-

Send offprint requests to: G. Aulanier

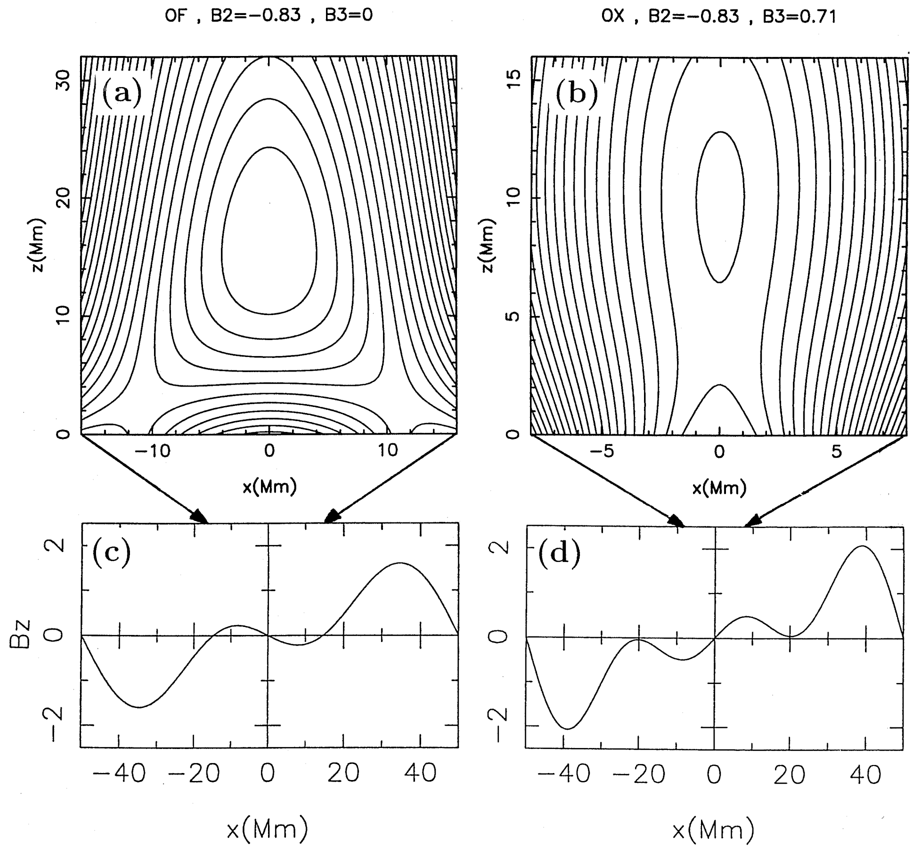

Fig. 1a–d The field lines for both twisted 2.5-D configurations that can support a prominence are shown in **a** and **b**, and their respective photospheric vertical magnetic field $B_z(z = 0)$ in **c** and **d**. **a** and **c** refer to the OF configuration, while **b** and **d** refer to a bipolar OX configuration. The first letter of the terminology refers to the topology at the top of the prominence, and the second at its bottom. The notation is derived from the local topology of the (B_x, B_z) components: O is given for an O-point, X for an X-point and F for a flat field line with two X-points on each side of the inversion line. Arrows indicate the relative size of the represented field lines **a**,**b** on the horizontal extension of the vertical field **c**,**d**.

nence is typically $<< 1$, so that magnetic tension is what keeps this overdense material from falling down. For this magnetic dips are needed. This point was first introduced by Kippenhahn & Schlüter (1957), though many advances have since been made in the study of dips in prominences (e.g. Priest et al. 1989).

A systematic overview of the different classes of magnetic equilibria is given by Aulanier & Démoulin (1998) (hereafter referred as Paper I). The magnetic field was described by the combination of a few harmonics of the linear force-free field. This method permits us to explore the large set of possible configurations. Only a few classes were found consistent with different observational constraints, especially the photospheric field distribution, the field inside the prominence, and the prominence morphology (with an emphasis on the underlying and the lateral feet). The best configurations found for a correct match with observations were twisted flux-tubes.

The purpose of this paper is to give a three-dimensional description of the magnetic field in filament channels, developing what has been done in Paper I. Our aim is to show that a twisted flux-tube which is perturbed by parasitic polarities is the correct magnetic configuration which supports prominences. We give a short summary of the method used in Sect. 2. The effect of parasitic polarities is described in Sect. 3. Then we justify our hypotheses, by comparison with an observed filament in Sect. 4. Sect. 5 is devoted to the topology of the field, and its evolution as the polarities move towards the photospheric inversion line. Sect. 6 emphasizes the importance of the quasi-separatrix layers, as we find an observational counterpart to them in chromospheric brightenings. Finally we summarize the results in Sect. 7.

2. The magnetic model

In this section, we explain the method used to compute the magnetic field in a filament channel. The ionisation degree and the value of the plasma β in prominences allow us to consider the ions and electrons as frozen in the magnetic field. Mercier & Heyvaerts (1977) have estimated the downward velocity of neutrals by ambipolar diffusion to a few m s^{-1}, which is much less than the free fall velocity (a few tens of km s^{-1}). As a consequence, neutrals are well coupled to charged particles, so that they are maintained in the prominence. The global prominence evolution (before eruption) can be described as quasi-static, due to the small plasma velocities observed (lower than sound and Alfvèn velocities). Furthermore, as the plasma β is of the order of 0.001 to 0.1, we can suppose in a first approximation that its effect on the magnetic field is negligible. Then the prominence configuration can be described with a force-free magnetic field. We choose to restrict ourselves to the linear force-free field (*lfff*), because it admits analytical solutions. We describe the main magnetic field by the combination of several 2.5-D harmonics, and we add small polarities using magnetic sources that also satisfy the conditions for the *lfff*.

2.1. The linear force-free field harmonics

The 2.5-D harmonics for the linear force-free field are given by the solutions of the equation:

$$\boldsymbol{\nabla} \times \boldsymbol{B} = \alpha \boldsymbol{B}\,, \tag{1}$$

with α = constant. The system of coordinates which is used here is cartesian. The $(x;y)$ plane defines the photosphere, the y axis referring to the prominence axis and z to the altitude. Hence, in 2.5-D, the field described by Eq. 1 can be expressed as a combination of harmonics (see Démoulin & Priest 1989, Aulanier & Démoulin 1998), given by:

$$B_x = -\frac{l\widetilde{B}_{(n_x)}}{k_x} cos(k_x x) e^{-lz}\,, \tag{2}$$

$$B_y = -\frac{\alpha\widetilde{B}_{(n_x)}}{k_x} cos(k_x x) e^{-lz}\,, \tag{3}$$

$$B_z = \widetilde{B}_{(n_x)} sin(k_x x) e^{-lz}\,. \tag{4}$$

where $\widetilde{B}_{(n_x)}$ is the amplitude of the harmonic numbered n_x,

$$k_x = 2\pi n_x / L_x\,, \tag{5}$$

$$l = \sqrt{k_x^2 - \alpha^2}\,. \tag{6}$$

It is noteworthy that for $\alpha > \alpha_{max}$ (defined as $\alpha_{max} = 2\pi/L_x$), e^{-lz} becomes imaginary. Then the amplitude of the first harmonic (followed by the higher ones as α increases) oscillates with height. This is unlikely to be physical for the description of a structure in equilibrium. So we restrict ourselves to $\alpha < \alpha_{max}$. In the followings, the values given for α are normalized to α_{max}. So the value of α in Mm^{-1} will be:

$$\alpha(\mathrm{Mm}^{-1}) = \alpha(\text{normalized}) \frac{2\pi}{L_x}\,, \tag{7}$$

and

$$\alpha_{max}(\text{normalized}) = 1\,. \tag{8}$$

It has been shown previously in Paper I that the combination of three harmonics $n_x = 1, 2, 3$ leads to different topologies for the magnetic field in 2.5-D. It has been shown as well that the best conditions for prominence support are found for large values of α, i.e. twisted flux-tubes.

2.2. The choice of the twisted flux-tube

Using a few harmonics is a suitable method for a systematic study of the parameter space: it permits to derive which magnetic configurations are compatible with the various observations. The best 2.5-D topology that satisfies the morphology of a prominence was referred to OF in Paper I. The notation is derived from the local topology of the B_x, B_z components: O for an O-point at the top, and F for a flat field line with two X-points on the side at the bottom (see Figs. 1a,c). This configuration extended to 3-D shows many advantages, especially for the appearance of underlying and lateral feet, as well as for comparison with Hanle effect measurement of the inclination of the field to the inversion line (see Bommier et al. 1994). In fact, it is the appearance of parasitic polarities in the low-field channel that leads to the presence of lateral feet. But a small number of harmonics naturally leads to many symmetries and periodicities, not only perpendicularly to the prominence axis, but also along the filament channel, which lead to very regular features that cannot be isolated or compared to observations. As a consequence the use of a small number of 3-D harmonics (as done in Paper I) permits to demonstrate the natural presence of prominence feet when parasitic polarities are present, but the study of the effect of a single polaritiy as well as the comparison of the model to the observations requires an extension of the model to more general configurations.

The purpose of this paper is to include small parasitic polarities around the inversion line, as it is observed in the filament channels (e.g. Martin 1990), in order to investigate the effect of isolated polarities, and to compare a modeled configuration to an observed filament. The configuration we choose for the unperturbed twisted flux-tube is OX, referring to an O-point at the top of the prominence, and an X-point at its bottom. This was the first twisted configuration proposed for prominence support (Kuperus & Raadu 1974). It has been shown in Paper I that the OX configuration does not describe a prominence correctly, especially because it shows no lateral feet, and its angle between the magnetic field and the inversion line is much too small (around 1^o). But we show in the following that the presence of parasitic polarities have an effect which modifies these limitations, leading to the observed features. For the rest of this paper, we will use a typical OX configuration described by:

$$\begin{array}{lll} \widetilde{B}_1 = 1 & \widetilde{B}_2 = -0.83 & \widetilde{B}_3 = 0.71 \\ L_x = 100\,\mathrm{Mm} & \alpha(\text{normalized}) = 0.99 & . \end{array}$$

These parameters are chosen from the so-called ($\widetilde{B}_2$, $\widetilde{B}_3$) diagrams (see Fig. 2 of Paper I) where the OX topology only appears for high α values. This gives a prominence that stands in altitude between $3.9\,\mathrm{Mm} \preceq z \preceq 10\,\mathrm{Mm}$, in a bipolar photospheric field (see Figs. 1b,d). The effect of increasing the value of α to closer to α_{max} is mainly to increase the height of the O-point at the center of the twisted flux-tube, but it does not much affect the lower regions. This dimensionless magnetic field is used in Sects. 3 and 5 to analyse theoretically the influence of parasitic polarities. It is worth noticing here that while the unperturbed flux-tube is of the OX type, the added parasitic polarities (Sect. 2.3) locally transform it to an OF configuration (see Sects. 3 and 4).

From paper I, the amplitude of these harmonics give a typical field strength in the filament of $B(\text{filament}) \simeq 0.75$, and from Fig. 1c,d the maximum value of the field in the strong bipolar component is $B(\text{bipolar}) \simeq 2$. In order to obtain B in Gauss, one has to multiply each amplitude of the harmonics by a factor f. The strength of the field in prominences is known to be around 5–20 G for quiescent prominences (Leroy et al. 1983) and up to 70 G for prominences of active regions (Kim, 1990). This gives approximately $7 \preceq f \preceq 90$.

2.3. Addition of parasitic polarities

We superpose parasitic polarities on the background field given by the harmonics, using the solutions of the *lfff* described in Démoulin & Priest (1992). This consists of putting one (or many) magnetic sources with an intensity C, at a distance d below the photospheric level. The expression of the magnetic field for a single source ($C = 1$, $d = 0$) is analytically given in their Eq. 15. The general effect of one source (C, d) on the photospheric vertical field can be summarized as the creation of a circular polarity of diameter $D \simeq d$, with a magnetic field intensity $B(\text{polarity}) \simeq C/d^2$.

The inclusion of such parasitic polarities, with appropriate parameters (C, d) fitted to the observed magnetogram, permits us to compare the model to the observed prominence features (Sect. 4 and Sect. 6). But before comparing to the observations we investigate the effect of one or two parasitic polarities. The parameters we use in the last case (Sect. 3) are $d = -5$ Mm and $C = 30$. This gives a parasitic polarity which has an approximate size of $D \simeq 5$ Mm (which is consistent with the observed polarities from Fig. 5), and a mean field of $B(\text{polarity}) \simeq 1.2$.

Choosing a value of $f = 40$ consequently leads to physical values for the magnetic field of $B(\text{filament}) \simeq 30$ G, $B(\text{bipolar}) \simeq 80$ G and $B(\text{polarity}) \simeq 48$ G. The flux of this computed polarity is then $\Phi(\text{polarity}) = 2\pi C \simeq 7.5\,10^{19}$ G cm^{-2}. These orders of magnitude fit well a typical observed magnetogram of a filament channel (see Fig. 5), as the strongest observed polarities have a maximum field intensity of 50–100 G.

3. How feet are linked to parasitic polarities?

We investigate the effect of parasitic polarities in the low field channel around a filament. We show how they naturally lead to the presence of dips along some field lines, on the side of the main prominence body. An evolution of the morphology of filaments as these polarities converge to the photospheric inversion line is proposed.

3.1. Scale height for the plasma filling the dips

In every figure, exceptions noted, that shows some dips in the field lines, we only represent the portion of field line which is supposed to be filled by dense plasma. For typical prominence physical parameters, the pressure scale height lies between 0.2 and 0.5 Mm (see Paper I). Assuming that the plasma remains optically thick (hence dark) on a few scale heights, we choose to draw the dips for a $H = 1$ Mm depth.

3.2. The effect of one parasitic polarity

We investigate here the effect of one parasitic polarity embedded in the main bipolar background field. Let us add a positive polarity source in the negative part of the background. Its effect is to create a local inversion line around itself. It is clear in Fig. 2a that only one part of this inversion line is privileged for the appearance of dips in the field lines. In fact, it is both the sign of α and the location of the source, whether in the positive or negative background, that lead to this segregation. From Fig. 2, there are several remarks that can be made just by looking at the morphology of the field lines.

Viewed along the prominence axis, the curvature radius of the dips look very small (see Figs. 2d-f). Hence, one may think that they could be easily observed. But this is not the case. A slight angle deviation of the viewpoint shows that these dips are in fact very flat and extended in the prominence axis direction. They can cover at least 10 Mm horizontally, while they are only 1 Mm high. This shows that they are really hard to observe. We will come back to this point in Sect. 4.

Another point is the existence of bald patches (Titov et al. 1993). Bald patches are characterized by field lines tangent to the photosphere. Bald patches are always present for the group of dips related to the parasitic polarity. Some others appear under the filament body, especially when the polarity is close to it. The unperturbed flux-tube normally extends in altitude between 3.9 Mm and 10 Mm (see Sect. 2.2), but there, it can be clearly seen on Figs. 2e,f that it reaches the photosphere. This effect leads to the appearance of one underlying foot, in addition to a lateral one.

Figs. 2a,d show a parasitic polarity located far away from the prominence. Though at that position dense matter can be supported against gravity, the local dips do not form a prominence foot, but they are separated from it. These dips may provide an explanation for darker fibrils and plagettes observed in the chromosphere (e.g. Martin et al. 1994). When the parasitic polarity is closer to the filament, its local dips form a continuous pattern with the dips of the filament body (see Figs. 2b,c,e,f). Hence such cases are a good candidate for the lateral feet of prominences. Furthermore, they follow the chirality rules found in Paper I: $\alpha > 0$ leads to a sinistral chirality. Finally, it can be said that the presence of lateral feet is due to a secondary inversion line caused by the presence of a parasitic polarity (or bipole) close to the principal inversion line, above which the prominence stands.

The main body of the prominence is also affected by the presence of this parasitic polarity. Even when it is relatively far away, the prominence top has risen (from 10 Mm to 14 Mm in Fig. 2a). The filament body is also somewhat distorted in its direction. When the polarity is closer (Fig. 2b), three effects are visible. First, the thin OX filament becomes thicker close to the polarity. Furthermore, the angle between the field lines and the inversion lines increases. These two points show that an OX configuration, which is initially unsatisfactory from various observational points of view becomes locally applicable for observed prominences. The third and last effect of the polarity on the filament body is to make it become very thin in its axis, on the opposite side of the local inversion line which creates dips above the polarity (Fig. 2c). The flux of the parasitic polarity overcomes that of the twisted flux-tube. It destroys locally the twisted configuration (at the lower part of Figs. 2b,c). But the figures show that there are some field lines with dips there. This is due to the fact that, as it has been emphasized before, the dips are very flat and extended along the prominence axis. Hence,

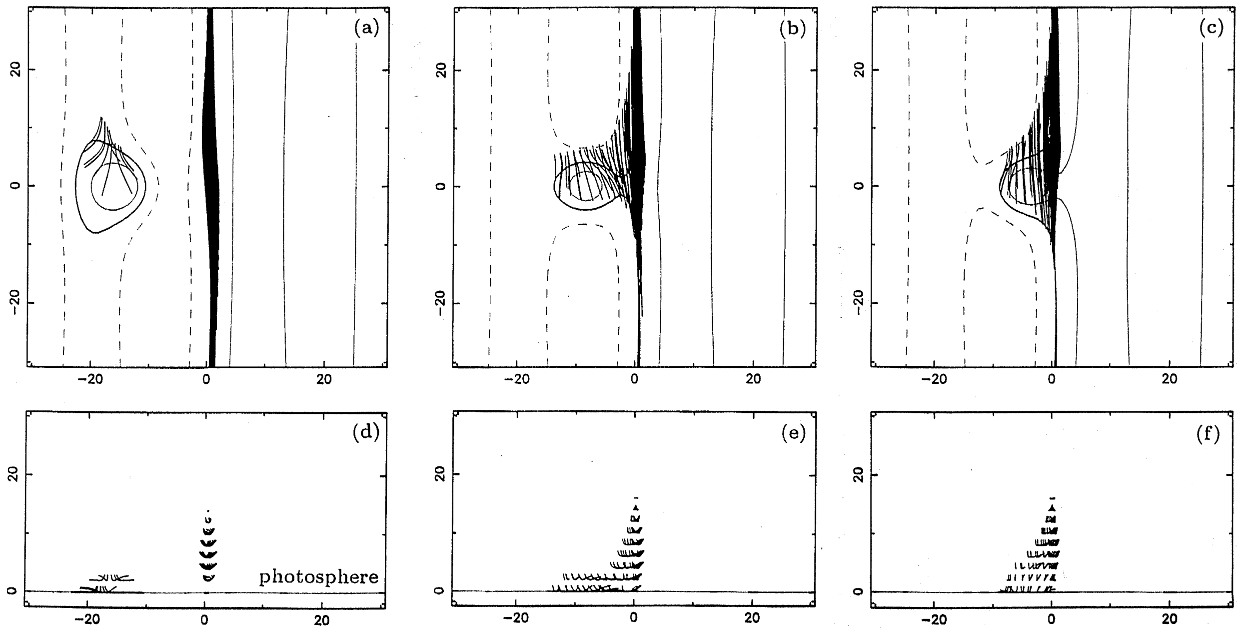

Fig. 2a–f A parasitic polarity is perturbing a bipolar OX prominence ($\alpha = 0.99$). The distance from the inversion line is 15 Mm in **a**,**d**, 8.5 Mm in **b**,**e** and 5 Mm in **c**,**f**. **a**,**b**,**c** are top views, and **d**,**e**,**f** are views in the prominence axis direction. The full (resp. dashed) lines correspond to isocontours of 0.3 and 2.1 (resp. negative values) for the photospheric vertical field. The inversion lines are represented in full thick lines. The portion of field lines, which dips are supposed to be filled with dense plasma on a depth of 1 Mm, are added. Note that $\alpha > 0$ leads to a sinistral configuration.

some field lines depart from the flux-tube and fill the gap where no dips are present.

Assuming that there are many parasitic polarities in observed filament low field channels (Martin 1990), one can state that all these local effects will become global on filaments. So a wide distribution of these polarities will contribute to the formation of many feet, to the thickening of the filament body, and to the increasing of the angle between the magnetic field and the prominence axis. Furthermore, it can be foreseen that for some configurations, especially in regions with isolated polarities, a filament may become very thin, or even more, interrupted.

3.3. Two polarities as a cancelling flux

A distinctive feature for the prominence feet which is well known to observers is the presence of cancelling flux, under the filament body, at the inversion line (e.g. Martin 1986). We show here the effect of two parasitic polarities in the main bipolar background field, facing one another, on each side of the inversion line (see Fig. 3). This configuration highlights some important effects which could not be observed with only one source.

Even when the cancelling polarities are facing each other as is shown in Figs. 3b,c, their associated lateral feet are shifted from one another; they do not face each other. As previously, there is only one part of each secondary inversion line, related to the parasitic polarities, which shows dips above it, and it is not the same on each side of the main inversion line.

Furthermore, it can be pointed out that there are some field lines that can pass from one foot to the other. This is only possible locally, close to the prominence body (Figs. 3b,c). This is because these field lines are not directly linked to the parasitic polarities, but to the distorted flux tube. In order to emphasize this point, it is also noteworthy in Fig. 3f that some field lines form arcades under the filament, crossing the inversion line, and having a dip on both sides. Hence, it is now clear that the configuration is locally OF (see Fig. 1a). So if one polarity only distorts the initial OX twisted flux tube, the presence of another one changes the local topology from OX to OF. This can only be achieved when the parasitic polarities are close enough to the flux-tube (typically 5 Mm to the principal inversion line). A more complete overview of the different types of field lines, and of the topology is given in Sect. 5.

3.4. Evolution in time

Parasitic polarities have been observed to converge to the inversion line above which the prominence stands (Martin 1990). What is shown in Fig. 2 and Fig. 3 does not come from an MHD evolution. It only shows different equilibria for different positions of the polarities for the same value of α. Though it may help to understand the modifications of the magnetic configuration as the polarities converge towards the inversion line. This scenario assumes that the field relaxes to its lower energy state (through a Taylor relaxation and with a given helicity) without a significant change of α. Though this should be further investi-

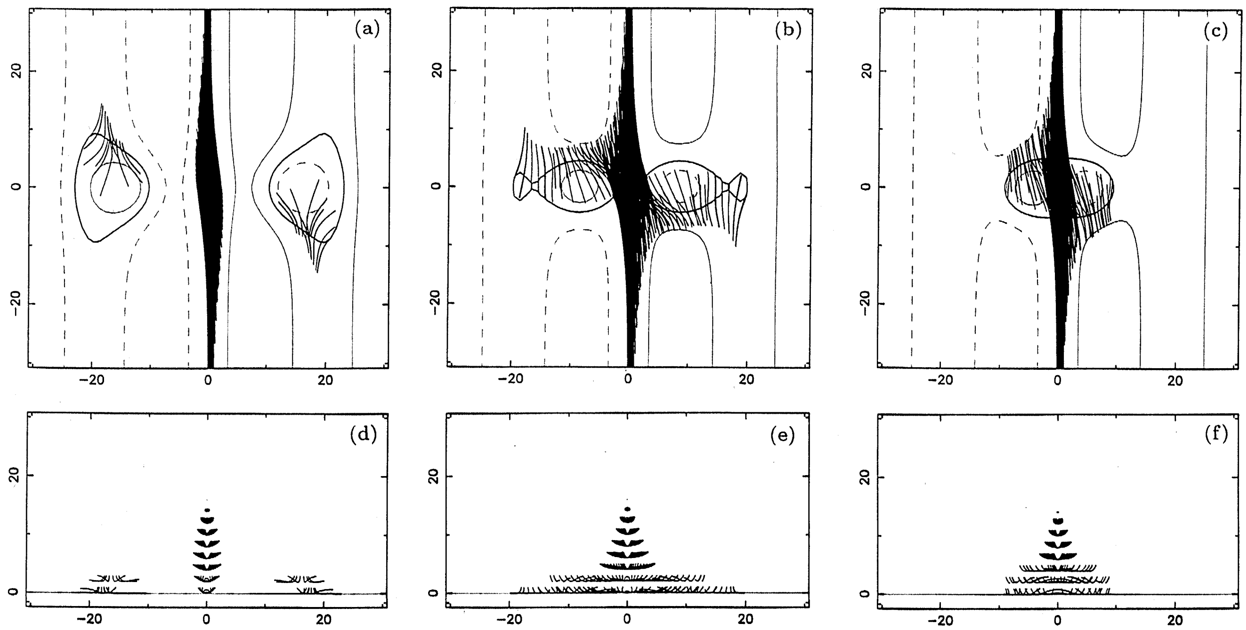

Fig. 3. Same as Fig. 2, except that there are two parasitic polarities facing each other on each side of the OX prominence.

gated through non-linear force-free field computations, as done by Browning et al. (1998) for a 2.5-D configuration, in the context of coronal heating. In our case, we believe that a Taylor relaxation in the full volume will fewly change the value of α, as the perturbed volume of the region (where the magnetic field is modified due to the presence of isolated parasitic polarities) is small compared to the full volume, while the magnetic field has a comparable strength.

Following the field lines that present a dip in Figs. 2 and 3 (a,d), and taking care of the photospheric-field linkage, it appears that they do not necessarily present a dip in (b,e) or (c,f), and vice versa. Taking into account the photospheric field linkage, it can be seen that the dips in (a,d) do not correlate with those in (b,e) or (c,f). Hence, some dips will disappear during the evolution, as some others will appear. During this process, it can be shown that some dips will rise upstream of the moving polarity, and that some will go down, reach the photosphere and disappear downstream of the polarity. So there can be matter flowing up and down from the photosphere, with the whole process driven by the motion of the parasitic polarity. It is clear on Fig. 2 and Figs. 3 (d,e,f) that dips appear higher and higher on the side of the prominence body as the polarities get closer to it. This process can bring mass to the filament. Its signature is vertical upwards dopplershifts near its borders, as observed by Mein et al. (1997).

It has been shown in Sect. 3.3 that when a pair of parasitic polarities come close enough to each other and to the main inversion line, the topology locally evolves from OX to OF. But numerical modelling of the MHD evolution will be needed to understand the passing from OX to OF. It has been numerically proven by Dreher et al. (1997) that a strong current density is likely to appear between two isolated cancelling polarities, driving reconnection, hence changing the topology. This kind of work should be extended to our case.

4. Comparison with observations

At this point, it becomes necessary to compare an observed filament with the model we propose for prominences. The filament has to be chosen in order to check every effect appearing for the previous theoretical cases. The major constraint is to have a filament which is quite straight, and the filament should not be too distorted, so that the main morphological features such as the feet, the body and the plagettes should be easy to identify. We use a filament observed on 25 September 1996 in Hα (see Fig. 4a) with the MSDP on the German VTT (Tenerife). More information specific to this observation are reported in Mein et al. (1997).

4.1. Magnetogram

The main argument of our model is that the magnetic field drives the whole structure of the filament. We have available a SOHO/MDI magnetogram for the normal component of the magnetic field (Fig. 5). It shows that the filament is situated in a very low vertical field region at the limit of the instrumental noise, with remarkable small polarities on either side of the filament. There are strong polarities further away from the prominence axis, showing a typical bipolar configuration.

A direct *lfff* extrapolation from the observed magnetogram does not permit to have a localized high sheared field (or even twisted) embedded in a potential arcade (see e.g. Schmieder et al. 1996). A non-linear force-free extrapolation would be required but no transverse-field measurements are available (in any case, the field strength is too low outside sunspots). With a

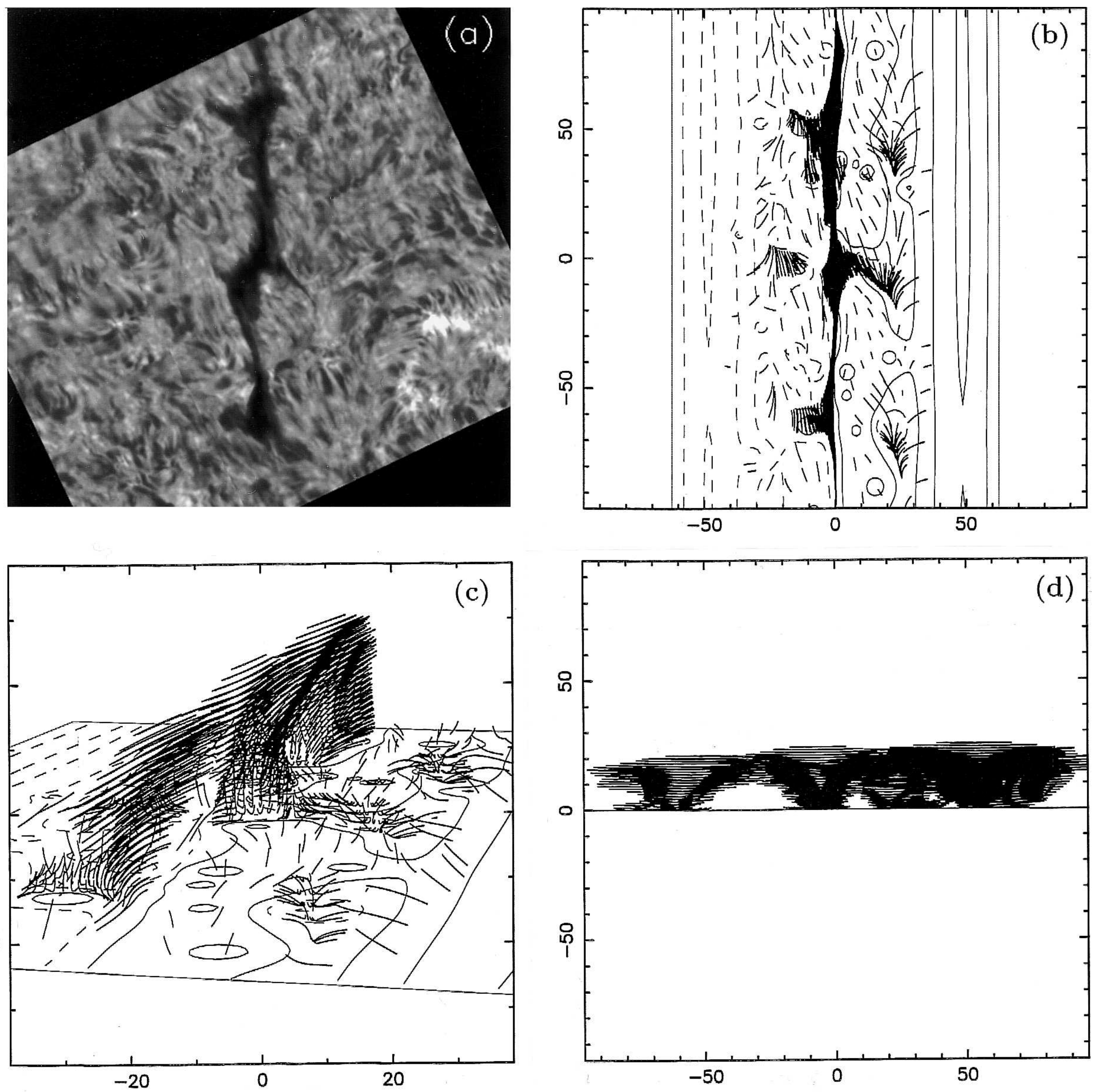

Fig. 4a–d Morphology of an observed prominence. **a** is a filament observed in Hα with the MSDP on the German VTT (Tenerife), on the 25 September 1996. **b**,**c**,**d** are different views of the modeled filament (resp. from the top, in 3-D and from the side as it would be observed on the limb). The full (resp. dashed) lines correspond to isocontours of 0.2, 1.0 and 2.0 (resp. negative values) for the photospheric vertical field. The scale of the axis is given in Mm. The thicker lines, where they are close to each other, represent the portion of field lines whose dips are supposed to be filled with dense plasma, on a depth of 1 Mm. These correspond to the filament and plagettes/dark fibrils. The other ones, in the filament channel represent the bottom of field lines, which correspond to Hα fibrils.

lfff we can only model the central part of the magnetic configuration and the *lfff* needs to be confined laterally. This is realized with a periodic field in the direction orthogonal to the filament (in the x direction for our purpose). So we have to construct a modelled magnetogram from the observations.

The MDI magnetogram shows that the filament is located inside a large-scale bipolar region. We then assume that there is a background bipolar field which creates an OX configuration, which is infinite in the direction of the inversion line. But we do not have any observational information about this possible twisted flux-tube. We choose to keep exactly the same amplitudes for the 2.5-D harmonics given in Sect. 2.2, as they represent a typical OX twisted configuration. It is possible to include a finite extension of the flux-tube along the filament axis (by using a Fourier transform in this direction), but this only introduces some effects at the end of the filament, while our goal is to study the prominence feet. We evaluate the horizontal extension of the bipolar field perpendicularly to the inversion line, from the distribution of the strong polarities in the observed magnetogram. We get $L_x = 125\,\mathrm{Mm}$. The value we choose for α has to stay very high (at least 0.9), so that there is indeed a flux-tube in this part of the $(\widetilde{B}_2, \widetilde{B}_3)$ diagram (see Paper I, Fig. 2

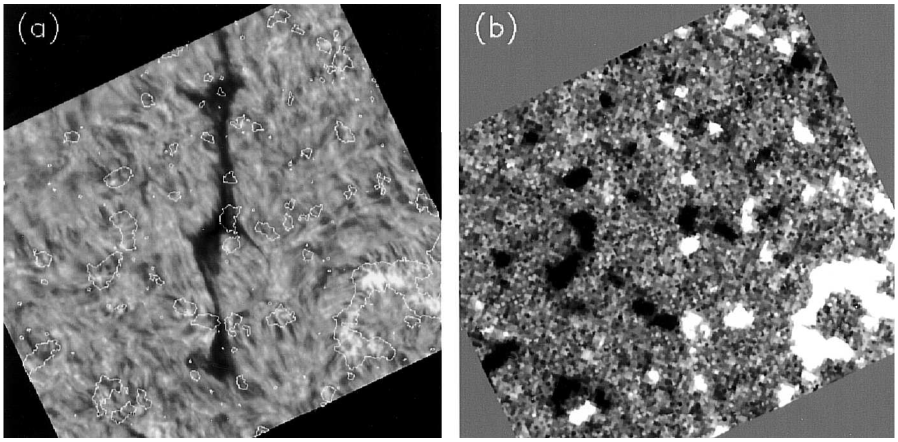

Fig. 5. **a** shows an overlay between the filament channel observed in Hα at 12:14 UT, and isocontours ($\pm$ 15 G) of the line-of-sight magnetic field observed with SOHO/MDI at 12:53 UT, on 25 September 1996. These observed values of the magnetic field can be considered as the normal component of the field to the photosphere, as the filament was around the center disc. The SOHO/MDI magnetogram is shown in **b**. White (resp. black) refers to positive (resp. negative) magnetic polarity.

for details). We will have to adjust its value to get the best match with the observed filament.

The principal argument developed in Sect. 3 for the morphology of the filament is the presence of parasitic polarities. So we have to keep the observed polarities in the filament channel as close as possible. This is done by modelling each polarity with a source with appropriate depth d and charge C (see Sect. 2.3). We show below that the polarities which play a key role in defining the filament structure are either the strong ones, or the faint ones with very low field surrounding them.

We finally have a magnetic configuration formed by a twisted flux-tube (OX configuration), and by a set of concentrated fields (as derived from the parasitic polarities given by a SOHO/MDI magnetogram). The validity of such a crude model can be disputed, but the results support the approach.

4.2. Results

We compute the magnetic field in a 3-D box above the constructed magnetogram for a given value of α. Then we draw the portion of the field lines which dips are likely to be filled with plasma. We also draw the bottom of a sample of field lines in the channel, which are likely to be observed as fibrils in Hα (see Paper I and Sect. 3.1). The comparison between the modelled field lines and the observed filament in Hα permits to choose the best value for α, so that both the modelled and the observed morphological features have the best correlation. Results for $\alpha = 0.995$ are shown in Fig. 4b. There is a good match for many morphological features: the lateral feet location, some dark fibrils in the filament channel, the local effects on the thickness of the filament, and the chirality pattern of the feet and fibrils. As found in Paper I, $\alpha > 0$ leads to a sinistral filament, which is consistent with the location of the observed filament in the southern hemisphere of the Sun. Moreover the shape of the prominence is also distorted by the polarities, especially in the top and in the central parts, where some parasitic polarities are present very close to the main inversion line.

The choice for the value of α is quite sharp as the filament body is very sensitive to its variations. The precision given is $(\delta\alpha/\alpha) \simeq 10^{-3}$. A small variation of α does not affect the feet and the lateral structures strongly. They can, in fact, be expressed as a combination of high-order 3-D harmonics of the *lfff* (high values of n_x and n_y), which are much less sensitive to α than low-order harmonics, such as the ones that create the OX flux-tube (formed by $n_x = 1, 2, 3$ and $n_y = 0$ harmonics). Hence the main flux-tube, i.e. the body of the filament, is the feature that shows the more sensitive morphological variations with α. Lower values of α progressively destroy the OX topology, so that only the feet are conserved, as the filament gets thinner. Higher values of α increase the size of the flux-tube, so that it gets higher and thicker. This is not relevant for our observed filament, as it is thin and almost interrupted. The best value is around $\alpha(\text{normalized}) = 0.995$, so $\alpha = 0.05\,\text{Mm}^{-1}$.

A 3-D perspective view of the dips and fibrils is presented in Fig. 4c. It shows how flat and extended the dips are, especially in the prominence body. The dips of the lateral feet clearly appear at low heights, and they join the underlying feet. Fig. 4d shows the filament as it would be observed from the limb. The presence of the underlying feet, and the void between them, are noteworthy. The horizontal features are only relevant for the step in z that we choose to draw the field lines. One can point out in Fig. 4a that the lower part of the filament is very thin, as in Figs. 2b,c. There are no more dips in this part of the magnetic configuration. But the field lines are so flat and well aligned with the filament axis that they fill this gap, so that dense plasma can still be present there. Fig. 4d shows these field lines viewed from the side. They give the illusion of a nicely continuous filament. Another observational consequence of this quasi-interruption of the filament body (other than the plasma low density), could be provided by the Hanle effect measurement of the angle between the field and the prominence axis. A very small value of this angle should be typical for these.

It is also noteworthy in Figs. 4c,d that some portions of the filament are darker than others. This is not due to any density enhancement, as we do not treat the plasma in our model, but simply draw field lines at dip locations, with a uniform distribution. It is only due to the projection views, which integrate the various shape of the dips, and the superposition of different structures, such as a foot or a plagette behind the filament. We propose that many observed brightness variations in filaments and prominences could simply be caused by such geometrical projection effects.

4.3. How much the flux-tube is twisted?

Dealing with an observed configuration, it is possible to look at its global shape. It can be shown by drawing the field lines that the shape of the flux tube defined in Sect. 4.1 is mostly perturbed by the parasitic polarities. But the number of turns per unit of length is almost unaffected by them. From Fig. 4, the length of the observed filament is about $L(\text{filament}) = 180\,\text{Mm}$. Furthermore, the field lines at the border of the computed flux-tube (the ones passing just at the top of the twisted configuration and at the bottom of the prominence) show a periodicity of $L(1\text{ turn}) \simeq 440\,\text{Mm}$. Hence the number of turns in the filament is:

$$N(\text{turn}) = \frac{L(\text{filament})}{L(1\text{ turn})} \simeq 0.4 \tag{9}$$

So the modeled flux-tube does not show such a big twist in the filament region. The field lines cannot even make one turn from one extremity of the prominence to the other one. This shows how difficult it is to observe the twist. One can state that such a configuration is unlikely to be kink-unstable (except if the twisted flux-tube extends for much longer than the filament).

5. Topology of a perturbed twisted flux-tube

The study of the topology of an infinite twisted flux-tube perturbed by one or two parasitic polarities shows the connectivity of the entire field lines, defining separatrices or quasi-separatrices, and it brings information on the morphology of the field lines. It highlights the differences between different groups of field lines which has been mentioned in Sect. 3.

5.1. The quasi-separatrix layers method

The generalization of the classical separatrices in 3-D naturally leads to the use of the quasi-separatrix layers or QSLs. Their intersection with the photospheric plane shows the location of the footpoints of field lines, whose connectivity changes drastically as one passes from one side of the QSL to the other. We use this method to study the topology in our modeled prominences. We refer the reader to Priest & Démoulin (1995) and Démoulin et al. (1996) for a discussion of the properties of their width, and of the basic characteristics of QSLs.

It is well known that strong currents can be generated at separatrices (i.e. zero-width QSLs; see Low & Wolfson 1988, Vekstein et al. 1991). But though the magnetic topology does not show any discontinuity at finite-width QSL locations, Démoulin et al. (1996) have shown that some strong currents could also be generated there, by photospheric displacements. Energy release is likely to be present at QSL locations. This has been proved by the presence of Hα kernels related to QSLs for different observed flares (see Mandrini et al. 1996, Démoulin et al. 1997 and Schmieder et al. 1997). While the evolution of the magnetic configuration is usually much more quiet around filament than in flares, we expect some low level of reconnection at the QSLs, due to slow photospheric motions. So an observational signature of energy release at the QSLs is also likely to be expected here.

5.2. One polarity

We use here exactly the same parameters as in Sect. 3.2: one parasitic polarity perturbates an infinite 2.5-D OX flux-tube. Dips are present above the parasitic polarity. As the polarity is far enough from the principal inversion line, these dips are in a distinct region from those of the twisted flux-tube (see Fig. 6a). But for a shorter distance, the QSLs have merged, and the OX topology is locally destroyed by the BP (bald patch, see Figs. 6b,c). There, the separator reaches the photosphere. It forms an underlying foot (resulting from the downward extension of the twisted flux-tube). That is why the filament becomes thicker in these locations (see Figs. 2b,c). As the parasitic polarity converges towards the inversion line, the lateral foot becomes attached to the underlying foot and to the filament body.

5.3. Two shifted polarities

We investigate here the configuration obtained with two parasitic polarities on either side of the inversion line, but shifted from one another by 30 Mm (typical size for supergranular cells), in such a way as if there were field lines going from one another. If Fig. 6d is quite similar to Fig. 6a, Figs. 6e,f definitely show a new topological feature. These configurations lead to the appearance of two underlying and two shifted lateral feet (above bald patches). We call this topology OF because the field lines present two dips on each side of the filament, as in 2.5-D OF configurations. The morphology of such a filament shows two separate underlying feet, shifted by 30 Mm, and the filament is interrupted or very thin between them. It is important to note that if the polarities were shifted in the other direction than in Fig. 6d,e,f, they would behave like two isolated parasitic polarities, as they are not magnetically linked (see Sect. 5.2 for the topology).

5.4. Two polarities in cancelling flux

5.4.1. BPs and QSLs

The cancelling flux configuration is treated last, though it is not the least, neither in importance nor in complexity. It can be seen, even from Fig. 6g, that the presence of two parasitic polarities facing each other from far away (30 Mm there) destroys locally the OX topology, forming a central BP. On both sides of the BP the separator reaches down to the photosphere. In this configuration one underlying foot is present above the central BP and it is separated from the two lateral feet (above lateral BPs).

The same is still valid, but another distinctive feature appears when the polarities are closer (see Fig. 6,h). It is due to the merging of the QSLs around each polarity with the ones related to the flux-tube around the main inversion line. In this

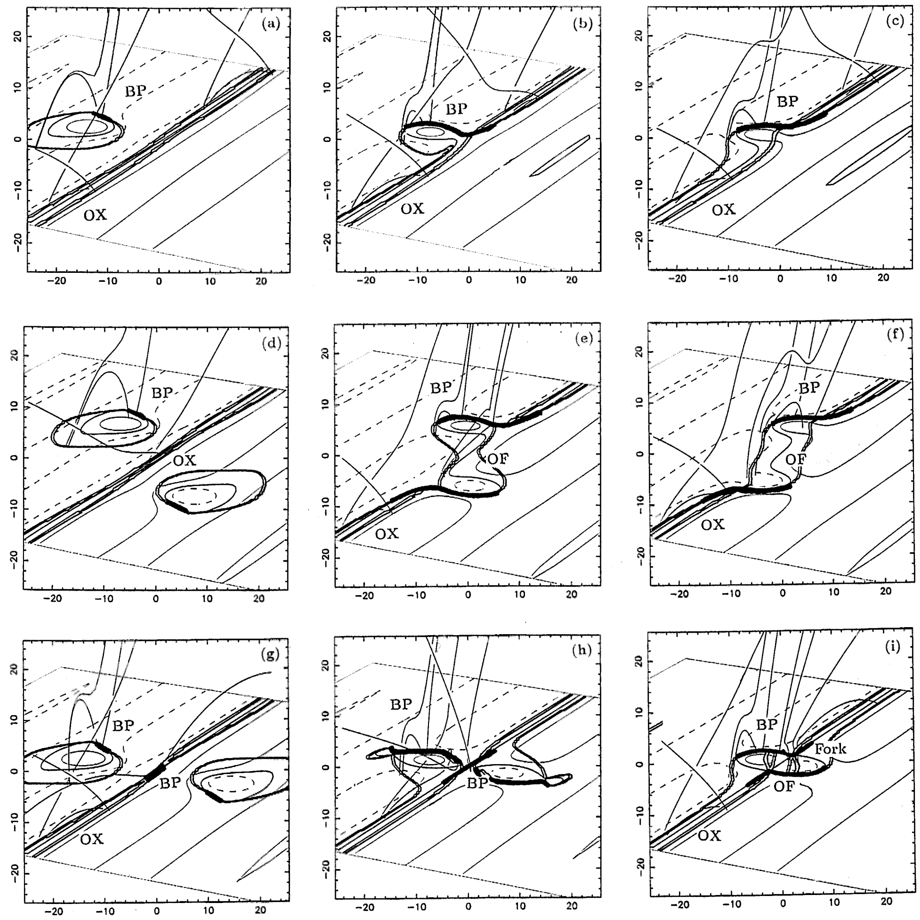

Fig. 6a–f Topology of the field around a twisted flux-tube perturbed by parasitic polarities. **a**,**b**,**c** refer to one polarity, **d**,**e**,**f** to two polarities shifted on each side of the inversion line, and **g**,**h**,**i** to two polarities converging face to face, as a cancelling flux. **a**,**d**,**g** correspond to a distance of 15 Mm from each polarity to the main inversion line, **b**,**e**,**h** is given for 8.5 Mm, and **c**,**f**,**i** for 5 Mm. The full (resp. dashed) thinner lines, on the photospheric plane, correspond to isocontours of 0.3 and 2.1 (resp. negative values) for the photospheric vertical field. The thin lines, on the photospheric plane, correspond to the inversion line. The thick lines correspond to the intersection of the quasi-separatrix layers (QSLs) with the photosphere. The thickest lines show the location of bald patches. The full lines in 3-D represent typical field lines for a given topology. The vertical extension is multiplied by 4, so that it is easier to see the field lines that would normally appear very flat. OX and OF are named from the corresponding 2.5-D configuration, BP relate to bald patches and Fork to the transition between BP and OF.

configuration the single underlying foot joins the two lateral ones.

When the polarities are even closer, things become quite tricky (see Fig. 6i). The detailed study of the evolution from Fig. 6h to Fig. 6i reveals that the central BP region splits in two, and its parts diverge from one another as the sources get closer. There some field lines with two dips appear; hence we have a local OF topology. The topology becomes complex: the intersection of QSLs with the lower boundary forms a square-like region with other QSLs on two sides. We call the QSLs which go deeper in the parasitic polarities simply Fork QSLs (from their shape). So the Fork topology marks the transition between OF and the BP of the polarities. This configuration changes the morphology of the prominence by separating the unique underlying foot (due to the previous central BP) into two distinct feet, with a small void between them. Each of the lateral feet then joins a different underlying foot. But this void is very small and local, compared to the ones produced by two shifted polarities. It would be more likely to be observed as an irregular single underlying foot.

5.4.2. Field line pattern

We now investigate more deeply the structure of the cancelling flux shown in Fig. 6i. The parasitic polarities are only 5 Mm from the main inversion line. There are two kinds of separators: the OX-BP and the BP-BP (Fig. 7a). The first one refers to a separator coming from infinity (a large value in the y direction for a finite-length configuration) and reaching down to the photosphere at the edge of the parasitic polarity. The second one joins the two BPs. It is formed by the intersection of the separatrices associated to the two BPs as found in another configuration by Bungey et al. (1996). It is a well known fact that reconnection is likely to take place at the separators (e.g. Gorbachev & Somov, 1988). Thus some activity is expected here in observed filaments.

Next we identify the typical field lines which have dips. There are five kinds of such field lines, reported in Fig. 7b. Field lines, called [1], are able to support the main prominence body. The other types ([2]-[5]) belong to the prominence feet. To avoid field line superposition, only one set is shown in Fig. 7,b but they are present above both BPs. The five kinds of field lines are:

– [1] field lines refer to the highest point in the prominence body. They are at the center of the twisted flux-tube. They only present one dip, just above the main inversion line. These dips are the most flat and extended ones along the prominence, and the angle between the field and the inversion line is very small.

– [2] field lines represent the bottom of the flux-tube. They have two dips, one on each side of the main inversion line. They represent the only link between the two lateral feet. These where named OF in the previous sections. A slight change in the flux of the parasitic polarities changes their geometry. So that

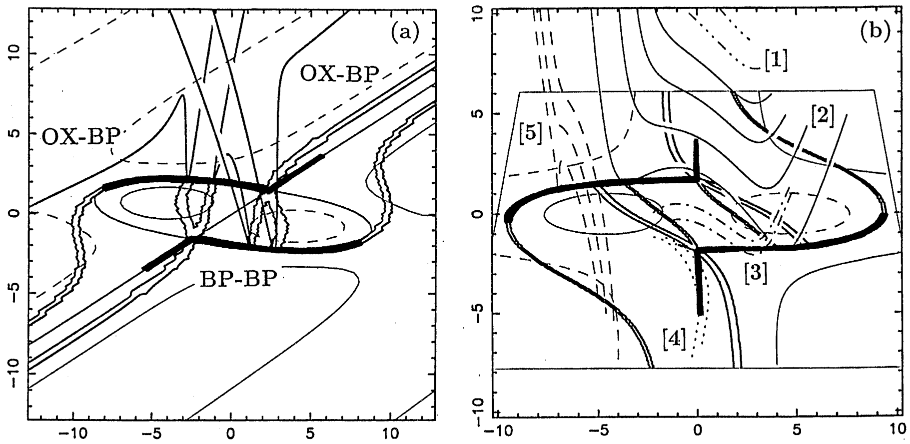

Fig. 7a and b Topology of the field around a cancelling flux under a twisted configuration. The three separators are reported in **a**, with a factor 4 of vertical extension. OX-BP correspond to the separators coming from the OX unperturbed flux-tube, to the parasitic polarity, where the topology is BP. The BP-BP separator corresponds to the local OF topology between the polarities; it joins two bald patches. The 5 different classes of field lines that have a dip are represented in **b**, with a factor 2 of vertical extension. The thick lines show the BP locations.

viewed from the side, as in Fig. 4d, some flow of matter could be observed passing from one foot to the other one.
– [3] field lines are topologically distinct from [2] by the BP-BP separator. They form small arcades in between the feet and have only one dip. They contribute to that part of the lateral feet that is the closest to the prominence.
– [4] field lines have almost the same shape as [3], but the projected view of Fig. 7b does not permit to see this point clearly. On one side they end in the positive polarity while on the other side they go in the twisted flux tube. Their dips are located above the split central BP, hence they support the underlying feet. Passing from [4] to [3] marks the step between the underlying and the lateral feet.
– [5] field lines are found above the BP created by the parasitic polarities. They contribute to the portions of the lateral feet that are far away from the prominence body, and very low in the atmosphere (see Fig. 3f). One can step from [5] to [4] by crossing the OX-BP separator.

5.4.3. Filament evolution

Assuming that we can pass continuously between the equilibria presented in Figs. 6g-i as the polarities converge, the foot morphology should evolve as follows: Initially, there are dark fibrils (plagettes) separated from the filament. As they converge and merge with the filament body, the filament locally rises (as shown by computing the dip locations), and the single underlying foot reaches down to the photosphere and extends horizontally along the prominence axis direction. As the lateral feet shrink, the underlying foot splits into two distinct ones, and magnetic arcades appear between them. These underlying feet progressively join the lateral ones. When the cancelling is complete, the lateral and the underlying feet, as the local enhancement of the height of the prominence, shrink back to the unperturbed twisted flux-tube.

6. Do QSLs have an observational counterpart?

It is now a well known fact that the QSLs are directly linked to the presence of Hα ribbons or kernels in flares (see Mandrini et al. 1996, Démoulin et al. 1997 and Schmieder et al. 1997). These are the signature of energy release via reconnection during the flares. It is also known that there are brightenings associated with filaments in Hα (e.g. Heinzel et al., 1995), but they are not systematic and their shape has not been determined. This is due to the fact that on the disk, the dense plasma of the filament is optically thick, and on the limb, the projection does not permit to see the underlying chromospheric region.

It is clear from Fig. 6 that QSLs are always associated with the presence of underlying and lateral feet. Both observations and theory find a much lower energy release in quiescent filament configurations than in flares. Then chromospheric lines such as Hα are not convenient for an observational signature of the QSLs. A line which is more sensitive to the energy release is required. We use one of the Calcium lines: the *y* line (Ca II, 8542 Å), which is also oberserved with the MSDP instrument (see Mein et al. 1997).

We show in Fig. 8 the comparison between the observed filament and the computed QSLs, for the same parameters given in Sect. 4 for the modeled filament. At first, the correspondence between QSLs and Calcium brightenings is not obvious, because this wavelength reveals the presence of strong magnetic flux in the network as well. These two kinds of brightenings can still be distinguished by using the following two properties. First, the brightenings associated to the network and the QSLs usually have different shapes. The network is composed of very small intense flux-tubes (e.g. Howard & Stenflo, 1972), so that the brightenings associated are more likely to form dashed features while the brightenings associated with QSLs are expected to show a more continuous, elongated and thin pattern (like flare ribbons). Second, the MDI magnetogram permits to identify the Ca II brightenings associated with strong polarities. Keeping only the brightenings not associated with the network, one can see in Fig. 8a that there are some brightenings associated with the QSLs of Figs. 8b,c. For example, the two arrows at the left of the filament on Figs. 8b,c point to nearly continuous and thin brightenings surrounding the filament feet. Similar brightenings, while less visible, are also present around the feet on the right side of the filament; they have a round shape characteristic

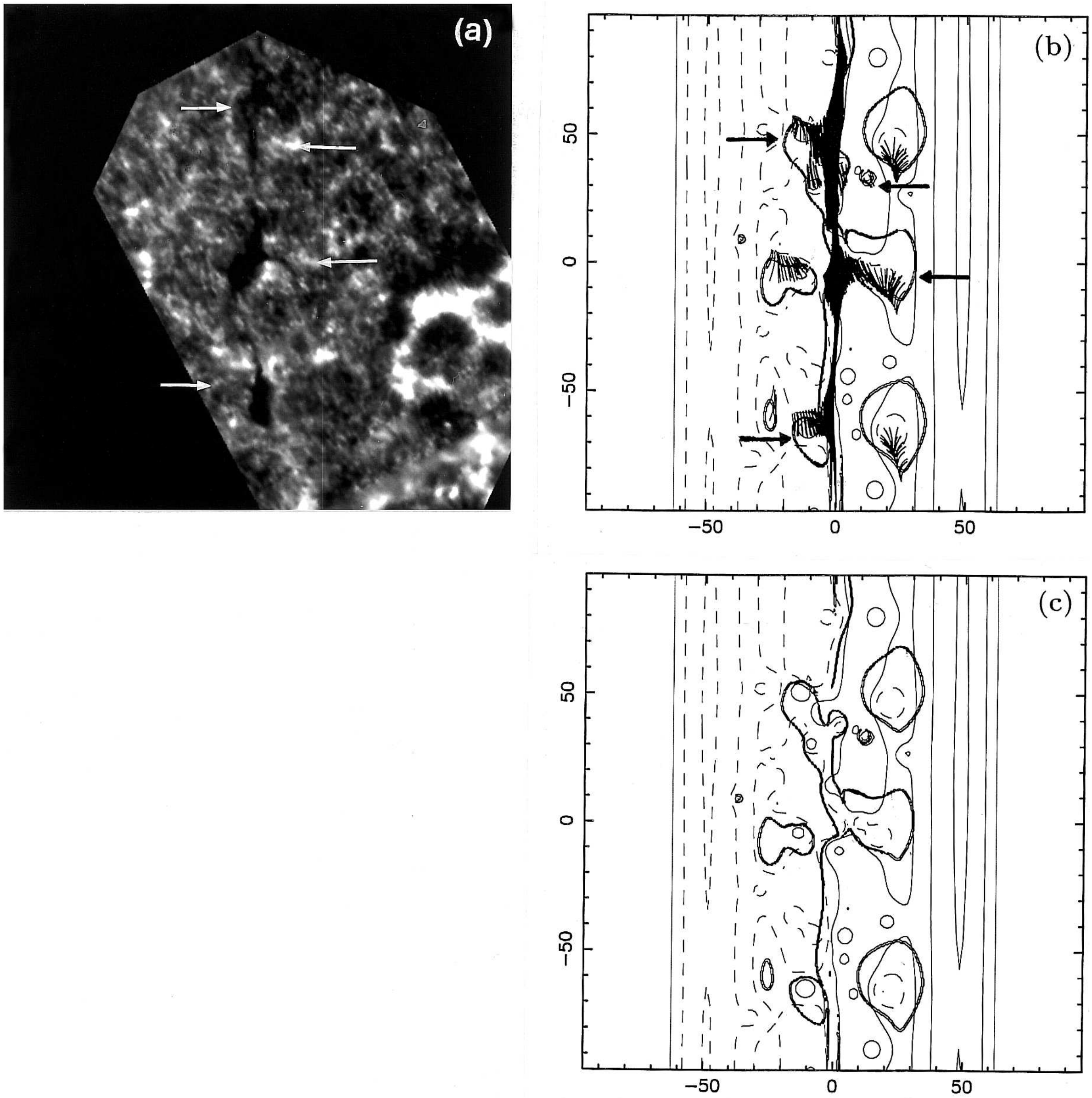

Fig. 8a–c Comparison of the QSLs locations with chromospheric brightenings. **a** shows the filament observed in the *y* line of the Calcium (Ca II, 8542 Å) with the MSDP on the German VTT (Tenerife), on the 25 September 1996. **b** is the top view of the modeled prominence (see Fig. 4) with QSLs included, and **c** only shows the QSLs. Arrows indicate the most obvious locations where there is a correlation between the lower part of the QSLs and the Ca II brightenings.

of the computed QSLs. These brightenings show indeed that there is energy deposit at these locations. The exact process of such heating is to be clarified, but it is likely to be linked with dissipation of the currents that can appear at the QSL locations.

7. Conclusions

The main hypothesis used in this paper is that dense plasma in prominences is supported against gravity by the magnetic tension of upwards-curved field lines. We have shown that a typical filament channel could be described, in terms of magnetic fields, by an OX twisted flux-tube for the main filament body. Furthermore the photospheric field presents a bipolar low vertical field channel. We have emphasized that perturbing this simple topology by parasitic polarities, naturally created some new dips, where dense matter is also likely to be present. These do not only lead to a vertical perturbation of the flux-tube, the effect of which is to show underlying feet structures, but also to the appearance of lateral features on the sides of the filament, such as lateral feet, dark fibrils and plagettes.

We have shown how the dip locations and the topology of the field depend on the distance of these parasitic polarities from the prominence axis, as well as on their relative locations. A complete study of the evolution of these configurations is far from the scope of this paper, though it would bring new information to what has been attempted here with the quasi-static approach. We have to point out the possibility of upward motions in the feet as the parasitic polarities converge to the main photospheric inversion line. Plasma motions are also likely to be present along the prominence axis, in the very flat field lines of the twisted flux-tube. Magnetic connections between two neighbour feet have been identified (this is a generalization of the OF configuration from 2.5-D to 3-D); it brings the possibility of mass exchange between two neighboring feet.

Another relevant point is that the unperturbed OX twisted flux-tube usually has an angle between the magnetic field and the prominence axis much too low compared to the results of Hanle-effect measurements. But the presence of parasitic polarities in the channel permits to have larger angles, consistent with the observations (locally the topology is changed from OX to OF). Thus we claim that these parasitic polarities are of major importance for understanding filament observations. The presence of an OF topology may have its origin in the convective region. Moreno-Insertis & Emonet (1996) have shown that only magnetic flux-tubes which are twisted can cross the convective region without being destroyed. The angle needed between the magnetic field and the flux-tube axis is consistent with magnetic measurements in filaments. Moreover, the central part of the flux-tube is more buoyant; as a result the twisted flux-tube is deformed to an OF topology (as in Fig. 1a of this paper, and in the figures in Moreno-Insertis & Emonet (1996)). Then, flux-tubes which emerge from the convective zone have the right shape to create lateral feet ! Obviously, one also needs to take into account that the super-granular cells have 3-D configurations with finite extension along the prominence axis (as opposed to the 2.5-D case). Though, this converging view between two different approaches is promising.

In paper I, we have shown that the model can interpret many of the well-known observations. Here, using observations of a particular filament, we confront more precisely the magnetic model with the observed shape of the filament. We model the coronal magnetic field using a SOHO/MDI magnetogram. We locate the magnetic dips and fill their bottom with dark material. The shape of the modeled filament, as the location of feet and dark fibrils, present a good correlation with Hα images. A relevant point is that the field lines in the modeled twisted flux-tube complete less than half a turn for the filament length. It implies that the detection of such a twisted configuration is very difficult during the quiescent phase. Moreover, overlaying coronal loops observed in in X-rays are not observed as helicoidal loops, but rather like sheared loops (Martin & Mc Allister 1995). During the evolution, magnetic helicity is accumulated in the magnetic configuration (Low 1996). When the twist is too high, an ideal instability occurs (Priest et al. 1989). Then the presence of twisted X-rays loops in erupting magnetic configurations (Manoharan et al. 1996, Pevstov et al. 1996, Rust & Kumar 1996) is compatible with the presence of a relatively low twist found in this work in the quiescent phase.

The computation of the quasi-separatrix layers, in this modeled prominence, has shown a plausible correlation with some brightenings as observed in Ca II (8542 Å). These brightenings are surrounding the feet of the filament. It confirms the foundations of the magnetic model. The presence of brightenings at QSL locations is interpreted as the consequence of magnetic reconnection. Then we propose that these brightenings have the same origin as the Hα flare kernels; the main difference being in the energy and time-scale involved.

Acknowledgements. The authors thank B. Schmieder for managing the SOHO/Yohkoh campaign in coordination with MSDP observations. Our ground-based campaign had received observing time under the International Time Program offered by the CCI of the Canarian Observatories and supported by the European Commission through the Access to Large Facility "Activity of the Human Capital and Mobility Program". It was also supported by the INSU and the GDR of CNRS "Magnétisme dans les étoiles de type solaire". We would like to thank J-M. Malherbe, B. Schmieder, J. Staiger, C. Coutard and R. Hellier for observing with us at the MSDP, and N. Mein for MSDP data reduction. LvDG acknowledges the research grant OTKA T17325. Finally the authors thank the referee for clarifying some points.

References

Athay R.G., Querfeld C.W., Smartt R.N., Landi Degl' Innocenti E., Bommier V., 1983, Solar Phys. 89, 3
Aulanier G., Démoulin P., 1998, A&A 329, 1125 (Paper I)
Bommier V., Leroy J.L., 1997, in D. Webb, B. Schmieder and D. Rust (eds.), IAU Colloq. 167, ASP Conference Series, in press
Bommier V., Leroy J.L., Sahal-Bréchot S., 1986, A&A 156, 79
Bommier V., Landi Degl'Innocenti E., Leroy J.L., Sahal-Bréchot S., 1994, Solar Phys. 154, 231
Browning P.K., Clegg J.C., Lothian R.M., 1998, in C. Alissandrakis and B. Schmieder (eds.), Proc. ASPE 98, ASP Conference Series, in press
Bungey T.N., Titov V.S., Priest E.R., 1996, A&A 308, 223
Démoulin P., Priest E.R., 1989, A&A 214, 360
Démoulin P., Priest E.R., 1992, A&A 258, 535
Démoulin P., Hénoux J.C., Priest E.R. and Mandrini C.H., 1996, A&A 308, 643
Démoulin P., Bagalá L.G., Mandrini C.H., Hénoux J.C. and Rovira M.G., 1997, A&A 325, 305
Dreher J., Birk G.T., Neukirch T., 1997, A&A 323, 593
Filippov B.P., 1994, Astron. Letters 20, 665
Foukal P., 1971, Solar Phys. 19, 59
Kim I.S. 1990, in V. Ruždjak, E. Tandberg-Hanssen (eds.), IAU Colloq. 117, Springer-Verlag, 49
Kippenhahn R., Schlüter A., 1957, Zs. Ap. 43, 36
Kuperus M., Raadu M.A., 1974, A&A 31, 189
Gorbachev V.S., Somov B.V., 1988, Solar Phys. 117, 77
Heinzel P., Kotrc P., Mouradian Z. and Buyukliev G., 1995, Solar Phys. 160, 19
Howard R.W., Stenflo J.O., 1972, Solar Phys. 22, 402
Leroy J.L. 1989, in E.R. Priest (ed.), *Dynamics and Structure of Quiescent Solar Prominences*, Kluwer Academic Publishers, Dordrecht, Holland, 77
Leroy J.L., Bommier V., Sahal-Bréchot S., 1983, Solar Phys. 83, 135
Leroy J.L., Bommier V., Sahal-Bréchot S., 1984, A&A 131, 33
Low, B.C., 1996, Solar Phys. 167, 217
Low, B.C., Wolfson R., 1988, ApJ 324, 574
Mandrini C.H., Démoulin P., van Driel-Gesztelyi L., Schmieder, B., Cauzzi G. and Hofmann A., 1996, Solar Phys. 168, 115

Manoharan P.K, van Driel-Gesztelyi L., Pick M., Démoulin P., 1996, ApJ 468, L73
Martin S.F., 1986, in A. Poland (ed.), *CPP NASA Conference*, C.P. 2442, 73
Martin S.F. 1990, in V. Ruždjak, E. Tandberg-Hanssen (eds.), IAU Colloq. 117, Springer-Verlag, 1
Martin S.F, Mc Allister A.H., 1995, IAU Colloq. 153, BAAS, 27, 961
Martin S.F., Bilimoria R., Tracadas P.W., 1994, in R. Rutten and C. Schrijvers (eds.), Solar Surface Magnetism, Kluwer Ac. Pub., 303
Mein P., Wiik J.E., Schmieder B., et al. 1997, in D. Webb, B. Schmieder and D. Rust (eds.), IAU Colloq. 167, ASP Conference Series, in press
Mercier C., Heyvaerts J., 1977, A&A 61, 685
Moreno-Insertis F., Emonet T., 1996, ApJ 472, L53
Pevtsov A.A, Canfield R.C., Zirin H., 1996, ApJ 473, 533
Priest E., Démoulin P., 1995, JGR 100, 23443
Priest E.R., Hood A.W., Anzer U., 1989, ApJ 344, 1010
Rompolt B., 1990, Hvar Obs. Bull. Vol. 14, 1, 37
Rust D.M., Kumar A., 1996, ApJ 464, L119
Schmieder B., 1990, in V. Ruždjak, E. Tandberg-Hanssen (eds.), IAU Colloq. 117, Springer-Verlag, 85
Schmieder B., Démoulin P., Aulanier G., Golub L., 1996, ApJ 467, 881
Schmieder B., Aulanier G., Démoulin P., van Driel-Gesztelyi L., Roudier T., Nitta N. and Cauzzi G., 1997, A&A 325, 1213
Titov S. Priest E.R., Démoulin P., 1993, A&A 276, 564
Vekstein G.E., Priest E.R., Amari T., 1991, A&A 243, 492